frontiers | Frontiers in Materials

ORIGINAL RESEARCH
published: 13 May 2022
doi: 10.3389/fmats.2022.850362

Facile Construction of Self-Healing Polydopamine-Based Composite Coating Protection of Copper From NaCl Solution

Wei Chen[†], *Juanjuan Fan*[†], *Yueyue Jiang, Shouting Li, Ye Ying* and Haifeng Yang**

The Education Ministry Key Lab of Resource Chemistry, Joint International Research Laboratory of Resource Chemistry, Ministry of Education, and Shanghai Key Laboratory of Rare Earth Functional Materials, College of Chemistry and Materials Science, Shanghai Normal University, Shanghai, China

Developing a sufficient composite organic inhibitor coating on the surface of metals is a promising strategy to improve the protection capability of metal materials from corrosive media. In this study, dopamine is polymerized into a polydopamine coating on a copper surface by embedding 8-hydroxyquinoline (denoted as PDA@8-HQ). The formation mechanism of PDA@8-HQ on the surface of copper is confirmed by X-ray photoelectron spectroscopy, Fourier transform infrared reflectance, and Raman methods. Electrochemical and field emission scanning electron microscopic results show that the PDA@8-HQ coating made with the addition of 8-HQ was 0.02 M and had the greatest inhibition efficiency (99.1%). When the optimal composite coating is damaged by external forces, self-healing capability could be obviously found due to generating insoluble complex species between corrosive products of copper ions and 8-HQ and the salt solution in the damaged region. This study provides feasibility for the construction of functional corrosion inhibitors on the metal surface.

Keywords: copper, polydopamine, 8-hydroxyquinoline, self-healing, inhibition of corrosion

OPEN ACCESS

Edited by:
Brahim El Ibrahimi, Université Ibn Zohr, Morocco

Reviewed by:
Omar Dagdag, Sidi Mohamed Ben Abdellah University, Morocco
Smrutiranjan Parida, Indian Institute of Technology Bombay, India

****Correspondence:***
Ye Ying
yingye@shnu.edu.cn
Haifeng Yang
haifengyang@yahoo.com

[†]These authors have contributed equally to this work and share first authorship

Specialty section:
This article was submitted to Environmental Degradation of Materials, a section of the journal Frontiers in Materials

Received: *07 January 2022*
Accepted: *07 March 2022*
Published: *13 May 2022*

Citation:
Chen W, Fan J, Jiang Y, Li S, Ying Y and Yang H (2022) Facile Construction of Self-Healing Polydopamine-Based Composite Coating Protection of Copper From NaCl Solution. Front. Mater. 9:850362. doi: 10.3389/fmats.2022.850362

INTRODUCTION

Nowadays, various metals, such as magnesium alloys, aluminum, carbon steel, and copper, are used in navigation and industrial fields (Jing et al., 2018; Wan et al., 2018; Feng et al., 2020; Zhang et al., 2021). Among them, copper, with its perfect mechanical workability, high strength at low temperature, good availability, excellent eminent electrical and thermal conductivity, has been widely applied in the fields of condenser pipes of ships, civilian pipes, and coastal power plant heat exchangers (Albinia et al., 2018; Qianga et al., 2018). However, as an active metal, copper tends to be corroded in the environment, especially in media containing chloride ions (Cl^-). Therefore, for preventing such corrosion, many anticorrosion methods have been developed, including a sacrificial cathode, chromate conversion coatings, self-assembly monolayers (SAMs), chromate-free corrosion inhibitors, and organic–inorganic hybrid coatings (Tavandashti et al., 2016; Grigoriev et al., 2017; Hou et al., 2017; Qian et al., 2017; Xu et al., 2018), among which organic barrier coatings have gained great interest due to their retention of properties of the metal component (Nestorson et al., 2007).

Organic polymer coatings are explored extensively due to their stability, low cost, and good mechanical strength (Jiang et al., 2013). Dopamine (DA) could form polydopamine (PDA) coating by self-polymerization, which easily attaches onto the surface of materials (Zhang Z et al., 2013; Chou et al.,

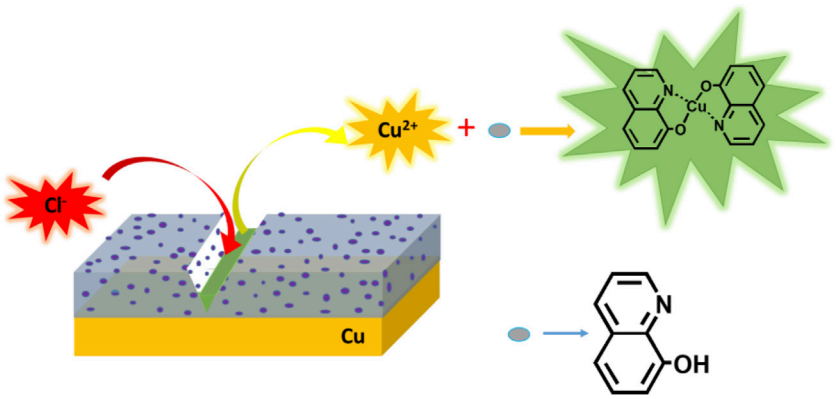

SCHEME 1 | Cartoon of the self-healing effect of PDA@8-HQ coating.

2016). However, in corrosive suppression field, some cracks in the PDA coating formed during self-polymerization would result in metal corrosion in chloride ion environments. Additionally, metals with PDA coating used in thermal cycling or damaged by mechanical scratch would increase coating crack and even peel off from the substrate (Li et al., 2017). Therefore, enforcement of PDA coating by introducing inhibitors is an alternative way.

Inhibitors entrapped into composite coating could diffuse out of coating to heal the cracks produced by external force factors (Zhao et al., 2019; Xu et al., 2021) and such composite coating is known as "smart" coating. The "smart" coating especially means that the damaged area can be self-repaired (Bhzadnasab et al., 2017). In the literature, some methods were reported to fabricate self-healing films: 1) electrospun coaxial fiber (Cheng et al., 2018), 2) ion-exchange organic resins (Zhao et al., 2018), 3) sol–gel (Caldas et al., 2017), 4) layered double hydroxides, 5) hollow SiO_2 (Chen et al., 2015), and silica/polymer hybrid nanotubes (Li et al., 2017). Typically, self-healing could be achieved *via* the following pathway: the self-healing coating containing linseed oil-loaded nanocapsules, potassium ethyl xanthate, benzotriazole (Mahmoudian et al., 2018), 1H-benzotriazole-loaded mesoporous silica sol–gel coating (Li et al., 2019), micro-arc oxidation/polymethyltrimethoxysilane composite coating (Cui et al., 2017), and polymer coating containing healing agent and microencapsulated catalyst. In view of those strategies, tedious preparation procedures are unavoidable, and the optimization of the corrosion inhibitor content and self-healing efficiency should be considered (Sumerlin, 2018).

Recently, in previous work, a study on functionalized multi-walled carbon nanotube-reinforced coating for metal protection was conducted (Jiang et al., 2021). Carbon nanotubes (CNT), due to their high specific surface area, good corrosion inhibition ability, good thermal stability, and good mechanical performance, were added in PDA coating, which exhibited better corrosion inhibition efficiency of 98.8% than pure PDA coating. The promising protection was probably owing to a strong interaction between PDA and functionalized CNT *via* hydrogen bonds, enforcing passive coating in a uniform and dense way. In this work, 8-hydroxyquinoline (8-HQ) as an effective inhibitor for metal corrosion in chloride solutions has been validated (Daradmare et al., 2016). We carefully study the possibility of embedding 8-HQ into PDA coating to fill the coating defects to improve inhibition efficiency. In **Scheme 1**, the self-healing procedure of the PDA@8-HQ coating at the copper surface is illustrated. When such coating is damaged by external forces, the inhibitor in the composite coating will be exposed. Free copper (II) ions will electrostatically adsorb (Gerengi et al., 2016) with 8-HQ and complex to repair the cracks caused by external factors, and then 8-HQ will complex with copper (II) to heal the cracks caused by external force factors, which forms clathrate of bis(8-hydroxyquinoline) copper [Cu $(HQ)_2$] (Zhang K et al., 2013), as indicated in **Supplementary Figure S1B**.

EXPERIMENT

Experimental Method

Dopamine hydrochloride (98 wt.% purity), Tris(hydroxymethyl) aminomethane (99.8% purity), 8-hydroxyquinoline (8-HQ, 98 wt.% purity), and ethanol (AR) were purchased from Sigma-Aldrich Corporation. Hydrochloric acid (AR) and sodium chloride (AR) were obtained from Shanghai Richjoint chemical reagents co., Ltd.

Pretreatment of Copper Electrode

Teflon sealed copper rod (99.999 wt.%) with an area of 0.0314 cm^2 was used as the observed electrode. First, to remove the oxide/hydroxide layer, the copper electrode was ground with 500- and 1,000-grit SiC papers. Then, 0.3 μm Al_2O_3 was used to polish the electrode surface. Finally, the polished copper surface was rinsed with deionized (DI) water (18.2 MΩ cm), pure ethanol, and deionized water successively to remove the loose oxides and alumina residue.

Surface Modification

1) The copper electrode was immersed into 2 mg ml^{-1} dopamine in 100 ml Tris–HCl (pH = 8.5) buffer solution for 12 h at room temperature. DA is therefore self-polymerized onto the copper surface, which is beneficial to the formation of a uniform and dense coating. The copper electrode with PDA coating, recorded

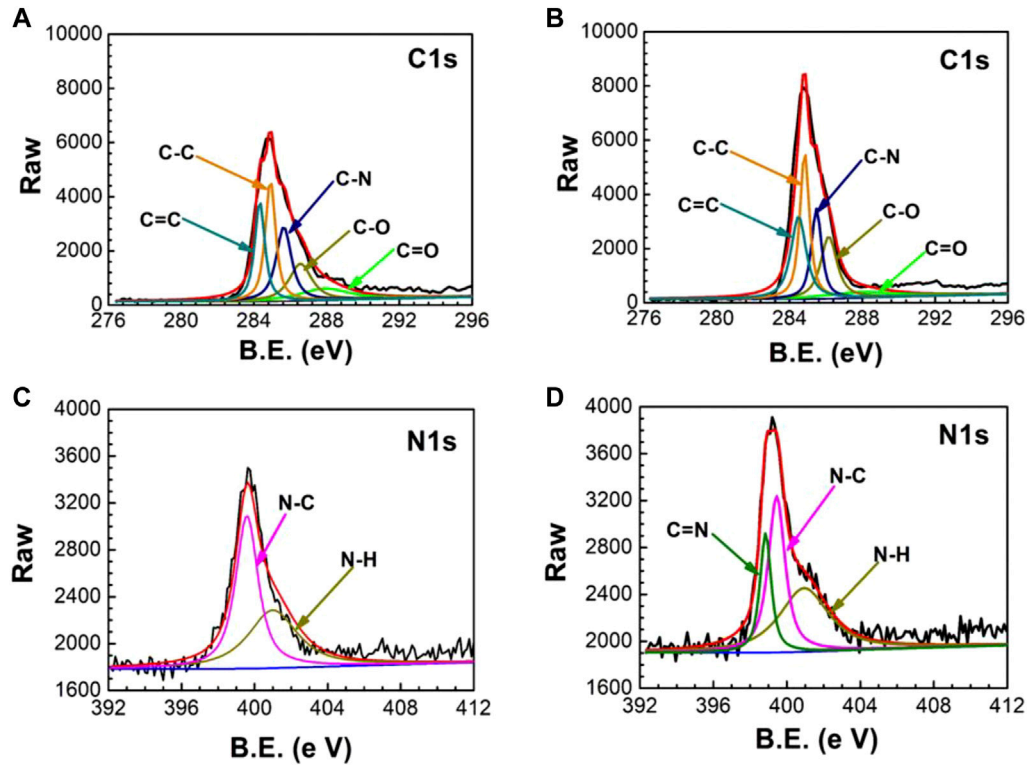

FIGURE 1 | XPS spectra of PDA@Cu **(A)** C 1s and **(C)** N 1s, and PDA@0.02 M 8-HQ@Cu **(B)** C 1s and **(D)** N 1s.

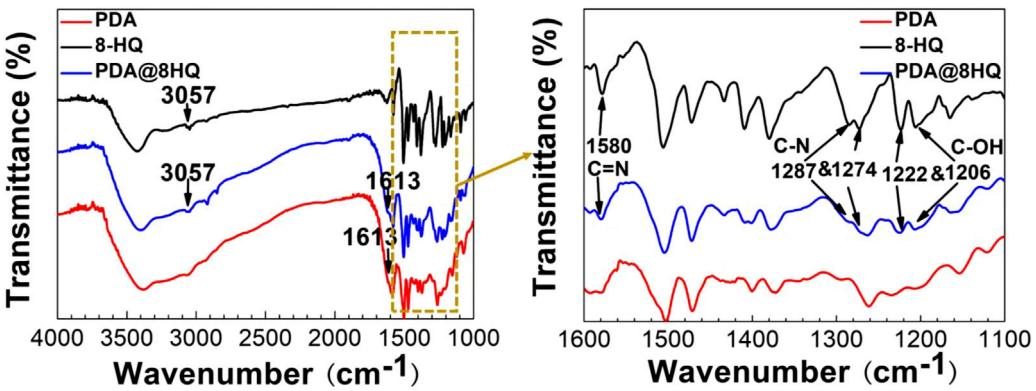

FIGURE 2 | ATR-FTIR spectra of different copper samples.

as PDA@Cu in the following text, was first rinsed with deionized water and then air-dried. The self-polymerization process of DA is shown in **Supplementary Figure S1A**.

2) The electrode was immersed in 0.02 M 8-HQ anhydrous ethanol solution for 12 h, rinsed with DI water, air-dried, and recorded as 0.02 M 8-HQ@Cu.

3) After that, 0.2 g DA was dissolved in 100 ml Tris–HCl (pH = 8.5) buffer with magnetic stirring at room temperature. Following that, 20 ml 8-HQ (with different concentrations) anhydrous ethanol solution was slowly added to dopamine solution under constant stirring. The final electrode (PDA@0.02M 8-HQ@Cu) was obtained after the bare copper electrode was immersed in the mixture solution for 12 h at room temperature.

Surface Characterization

The composition of the coating was characterized using X-ray photoelectron spectroscopy (XPS, PHI 5000 VersaProbe,

TABLE 1 | Bond composition and content of C = C, C-C, C-N, C-O, and C = O of C 1s.

Sample	Bond content (at%)				
PDA@Cu	C = C 20.69	C-C 22.94	C-N 21.73	C-O 18.71	C = O 15.93
PDA@8-HQ@Cu	C = C 22.60	C-C 24.03	C-N 19.39	C-O 20.04	C = O 13.94

Japan). It provided 1,486.6 eV photons using an Al Ka X-ray source (40 W, 15 KV). The test voltage and the base pressure of the analysis chamber were set at 6×10^{-7} Pa and 2×10^{-8} Pa, respectively. The coatings of PDA@Cu and PDA@0.02M 8-HQ@Cu were scraped off from the copper surface to conduct structural characterization by FTIR (Thermo Fisher Nicolet iS5, United States). The FTIR spectral range of 500–4,000 cm^{-1} was recorded with 4 cm^{-1} resolution in the transmission mode.

Raman spectra were collected using a confocal micro-Raman spectrometer (Super LabRam II system, Dilor, France). The laser and detector were 632.8 nm He-Ne laser and multichannel air-cooled 1,024 × 800 pixels charge-coupled device, respectively. The laser power, pinhole, and slit for Raman measurements were set at 5 mW, 1,000 μm, and 100 μm, respectively. Each Raman spectrum was acquired by 10 s three times and was calibrated using a silicon line (519.2 cm^{-1}).

The morphologies of electrodes were taken at 5 kV acceleration voltage by scanning electron microscopy (SEM, Hitachi S-4800).

Electrochemical Test

To observe the electrochemical behaviors of the electrodes with coatings, by using a VersaSTAT4 electrochemical workstation (AMETEK Princeton Applied Research), OCP, EIS, and Tafel polarization curves were measured in 3.5 wt.% NaCl aqueous solution. A conventional three-electrode system was used, with copper, Pt wire, and saturated calomel electrode (SCE) as the working, counter, and reference electrodes. In detail, the electrodes were kept in the NaCl solution for 10,000 s before EIS tests to obtain a steady state of OCP. The EIS experiment was carried out in the range from 100 kHz to 0.01 Hz with an AC amplitude of 10 mV. The electrochemical polarization curve was acquired at an open-circuit voltage of OCP ± 0.25 V (vs. SCE) with a scan rate of 1 mV s^{-1}.

Evaluation of the Self-Healing Properties

Bare copper, PDA@Cu, 8-HQ@Cu, and PDA@8-HQ@Cu specimens were scratched to expose the metallic substrates by using a ceramic knife (Analytik Jena). The scratched specimens were immediately immersed in 3.5 wt.% NaCl corrosive solution. The scratched portions of copper electrodes with and without treatment of corrosive media were observed using FE-SEM (Hitachi S-4800) and energy-dispersive X-ray (EDS) microanalysis (Hitachi S-4800).

Bare Cu and modified coppers were scratched and corroded in 3.5 wt.% NaCl solution for 10 h. Then linear sweep voltammetry (LSV) was performed by a VersaSTAT4 electrochemical workstation to evaluate self-healing behavior in three-electrode electrochemical cells. The potential range was from 0 to 1.0 V, and the scan rate was set at 50 mV/s (Bernsmann et al; Park and Braun., 2010, 2011; Johansen et al., 2012).

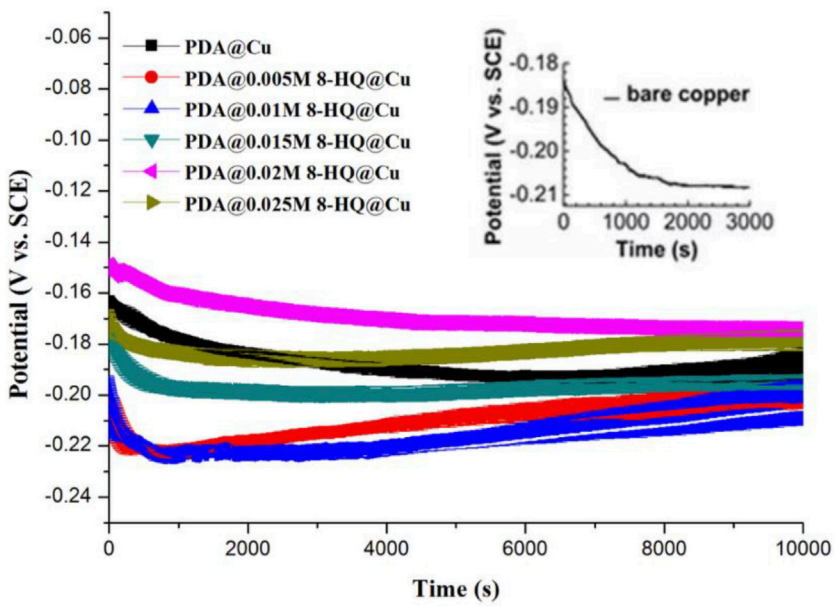

FIGURE 3 | Open circuit potential versus time of different copper samples recorded in 3.5 wt.% NaCl aqueous solution (The error means a standard deviation of three measurements. OCPs of bare Cu, PDA@Cu, and concentration of 8-HQ in 0.005 M, 0.01 M, 0.015 M, 0.02 M, and 0.025 M are –0.209 ± 0.003, –0.196 ± 0.002, –0.202 ± 0.004, –0.198 ± 0.003, –0.191 ± 0.003, –0.172 ± 0.002, and –0.187 ± 0.001 mV (vs. Ag/AgCl, 3 M KCl), respectively).

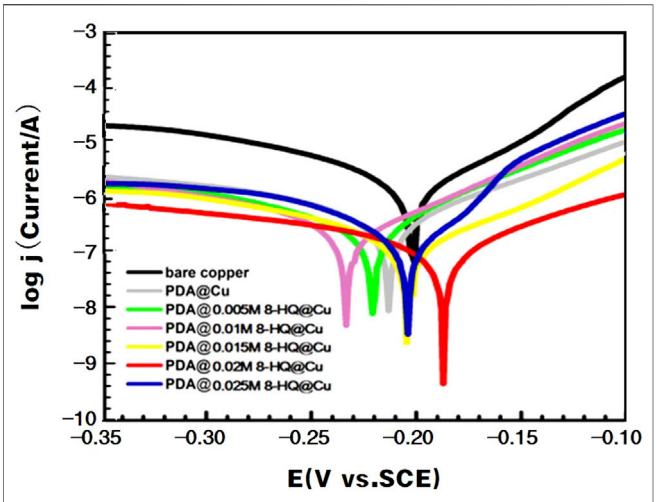

FIGURE 4 | Anodic and cathodic polarization curves of different copper samples recorded in 3.5 wt.% NaCl aqueous solution.

RESULTS AND DISCUSSION

Composition of Surface

The successful preparation of PDA@0.02M 8-HQ@Cu is confirmed by XPS and ATR-FTIR. **Figures 1A,B** show C 1s and N 1s XPS spectra of PDA@Cu and PDA@0.02M 8-HQ@Cu. From **Figure 2**, the contents of various C species are given in detail in **Table 1**. Some obvious differences could be found in C=C, C-C, C-N, C-O, and C = O groups after the introduction of 8-HQ, for PDA@0.02M 8-HQ@Cu in comparison with PDA@Cu. Direct evidence of the existence of 8-HQ in the composite coating could be offered *via* the comparison of the N 1s spectra. As shown in **Figure 2C**, N-C (399.7 eV) and N-H (400.9 eV) groups are attributed to PDA modified at the Cu surface, while in **Figure 2D**, the appearance of the C = N (398.7 eV) group in PDA@0.02M 8-HQ@Cu indicates the successful dopant of 8-HQ into PDA coating.

To further ascertain the structure of the coating, the FTIR experiment was conducted. As shown in **Figure 1**, the FTIR spectrum of 8-HQ presents a peak of C-H stretching at 3,057 cm^{-1}, two bands at 1,287 and 1,274 cm^{-1} correspond to C–N stretching, and a peak at 1,580 cm^{-1} is due to C = N stretching (Luo and Mather., 2013; Mahmoud et al., 2009), and the peaks at 1,222 and 1,206 cm^{-1} are also from C-OH stretching of 8-HQ (Daradmare et al., 2016). All corresponding bands are observed in the FTIR spectrum of PDA@0.02M 8-HQ coating. Additionally, as compared with the FTIR spectrum of PDA, a new band at 1,613 cm^{-1} occurring in the FTIR spectrum of PDA@0.02M 8-HQ coating is assigned to the superposition of phenylic C = C stretching (Liu et al., 2013), and intermolecular hydrogen bonds in PDA present a broad band in the 3,000- to 3,400-cm^{-1} region (Jiang et al., 2013). The previous FTIR investigation depicts the successful formation of a composite coating of PDA and 8-HQ at the copper surface.

Similarly, the Raman experimental results could also show the coating formation. From **Supplementary Figure S2**, Raman spectra of PDA@0.02M 8-HQ@Cu present a peak at 950 cm^{-1} from 8-HQ and two peaks at 1,382 and 1,603 cm^{-1} from PDA.

Open Circuit Potential

Recorded in 3.5 wt.% NaCl solution, **Figure 3** shows the curves plotted by open circuit potential (OCP vs. SEC) versus time for bare copper, PDA@Cu, and different PDA@8-HQ@Cu formed by changing the amount of 8-HQ. OCPs of bare Cu, PDA@Cu, and PDA@8-HQ@Cu with different concentrations of 8-HQ (i.e., 0.005 M, 0.01 M, 0.015 M, 0.02 M, and 0.025 M) are −0.209 ± 0.003, −0.196 ± 0.002, −0.202 ± 0.003, −0.198 ± 0.003, −0.191 ± 0.003, −0.172 ± 0.002, and −0.187 ± 0.001 mV, respectively. Obviously, the low OCP value of PDA@Cu is due to the defects in PDA coating, which could be observed in the SEM image (**Supplementary Figure S3**). From another aspect, some cracks in the PDA coating formed by self-polymerization would result in the occurrence of metal corrosion in chloride ions. By introducing an inhibitor (8-HQ) to synthesize a composite coating, the PDA coating with 8-HQ at the copper surface could dramatically prevent the attack of chloride ions, and the OCP value is relatively higher due to the defects filled by 8-HQ. In **Figure 3**, the OCP values first shift to the anodic direction and then to the cathodic direction with the increasing 8-HQ concentration. The RSD results in **Figure 3** are acquired by three measurements.

Due to external factors, the inhibitor in the composite coating will be exposed, and the free copper (II) ions will electrostatically adsorb with 8-HQ and complex to repair the cracks caused by external factors. Then, 8-HQ will complex with copper (II) to heal the cracks caused by external force factors. The test results showed that the corrosion inhibition effect of the coating is bad at low concentrations. The optimal concentration of 8-HQ to stuff the defects in the coating is 0.02 by observation of OCP at a more positive value, presenting the best anticorrosion ability. When a lower concentration of 8-HQ was used, the coating defects could not be filled completely, and when the 8-HQ concentration was

TABLE 2 | Corrosion parameters obtained from potentiodynamic polarization curves for different samples in 3.5 wt.% NaCl aqueous solution (The error means a standard deviation of three measurements).

Sample	$^{-}E_{corr}$ (V vs.·SCE)	j_{corr} (μA cm^{-2})	$^{-}\beta_c$ (V·dec^{-1})	β_a (V·dec^{-1})	η (%)
Bare copper	0.191 ± 0.002	0.776 ± 0.005	10.7 ± 0.86	23.1 ± 1.12	—
PDA@Cu	0.204 ± 0.004	0.129 ± 0.003	17.0 ± 1.51	18.7 ± 1.67	83.38
PDA@0.005M 8-HQ@Cu	0.215 ± 0.004	0.089 ± 0.004	11.6 ± 0.79	27.4 ± 0.98	88.53
PDA@0.01M 8-HQ@Cu	0.227 ± 0.003	0.044 ± 0.002	19.6 ± 0.94	37.6 ± 1.42	94.33
PDA@0.015M 8-HQ@Cu	0.201 ± 0.005	0.023 ± 0.003	49.3 ± 2.72	63.7 ± 2.71	96.78
PDA@0.02M 8-HQ@ Cu	0.184 ± 0.003	0.0071 ± 0.002	37.4 ± 1.73	97.2 ± 1.85	99.09
PDA@0.025M 8-HQ@ Cu	0.197 ± 0.005	0.0557 ± 0.004	21.3 ± 1.67	49.6 ± 2.98	92.82

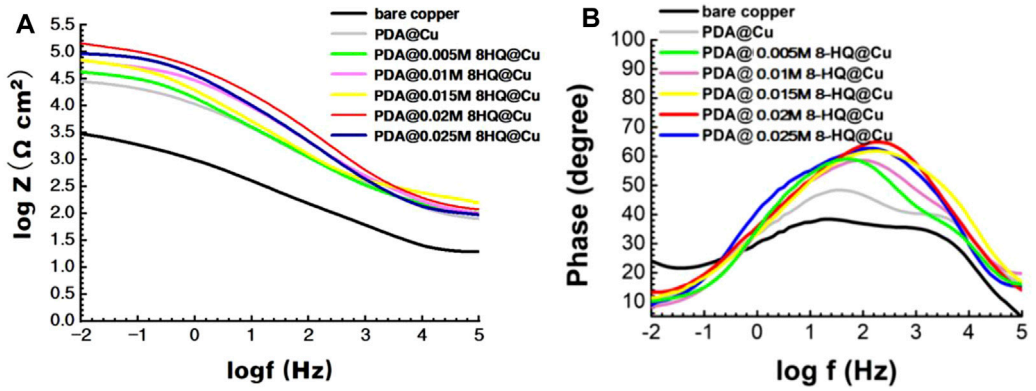

FIGURE 5 | Bode **(A)** and phase angle **(B)** plots for different copper samples recorded in 3.5 wt.% NaCl aqueous solution.

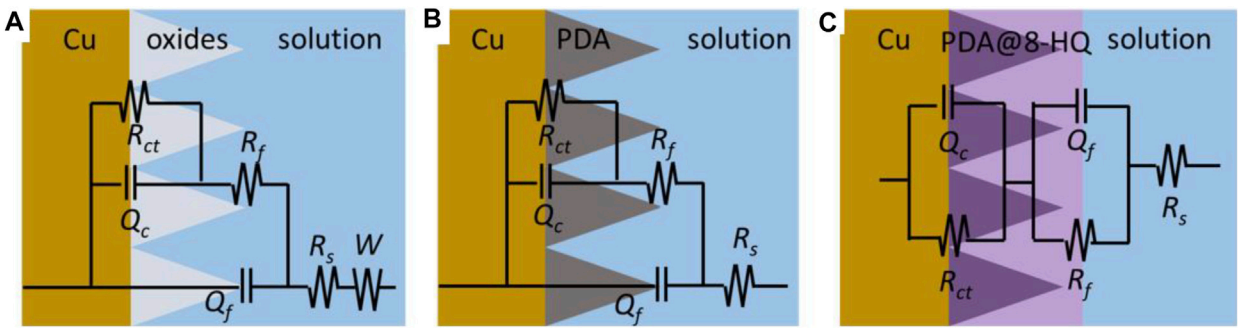

FIGURE 6 | Electrochemical equivalent circuits simulated for the impedance of the **(A)** bare copper, **(B)** PDA@Cu, and **(C)** PDA@8-HQ@Cu.

TABLE 3 | Electrochemical parameters calculated from EIS measurements for different samples in 3.5 wt.% NaCl aqueous solution (The error means a standard deviation of three measurements).

Sample	R_s (Ω cm^2)	$R_f \times 10^3$ (Ω cm^2)	Q_f $Y_0 \times 10^{-4}$ (Ω^{-1} cm^{-2}·S^n)	n_1	W $Y_0 \times 10^{-3}$ (Ω^{-1} cm^{-2}·S$^{0.5}$)	Q_c $Y_0 \times 10^{-4}$ (Ω^{-1} cm^{-2}·S^n)	n_2	$R_{ct} \times 10^3$ (Ω cm^2)	η (%)
Bare copper	0.58 ± 0.005	0.001 ± 0.00001	1.96 ± 0.02	0.86 ± 0.001	541 ± 4	117 ± 3	0.484 ± 0.03	0.075 ± 0.0006	—
PDA@Cu	2.08 ± 0.16	0.01 ± 0.002	0.960 ± 0.056	0.73 ± 0.001	—	7.20 ± 0.05	0.530 ± 0.03	0.97 ± 0.03	92.27
PDA@0.005M 8-HQ@Cu	2.22 ± 0.12	1.011 ± 0.01	2.30 ± 0.15	0.70 ± 0.003	—	29.58 ± 0.21	0.6325 ± 0.04	1.64 ± 0.04	95.43
PDA@0.01M 8-HQ@Cu	1.76 ± 0.14	0.726 ± 0.03	2.302 ± 0.17	0.77 ± 0.005	—	2.12 ± 0.06	0.6599 ± 0.03	2.05 ± 0.05	96.34
PDA@0.015M 8-HQ@Cu	1.87 ± 0.18	2.123 ± 0.04	5.783 ± 0.23	0.64 ± 0.004	—	1.61 ± 0.01	0.7558 ± 0.05	0.74 ± 0.01	89.86
PDA@0.02M 8-HQ@Cu	2.51 ± 0.17	0.857 ± 0.03	9.360 ± 0.32	0.80 ± 0.006	—	2.90 ± 0.02	0.6618 ± 0.02	3.10 ± 0.04	97.58
PDA@0.025M 8-HQ@ Cu	1.53 ± 0.11	2.632 ± 0.05	2.887 ± 0.19	0.70 ± 0.002	—	2.717 ± 0.03	0.7559 ± 0.02	0.50 ± 0.02	85.00

excessive, 8-HQ would precipitate in the crystal form during the reaction, which also affected the integrity of the coating.

Electrochemical Polarization

The potentiodynamic polarization curves (**Figure 4**) of the bare and modified copper electrodes were acquired in 3.5 wt.% NaCl aqueous solution. The resultant electrochemical parameters are listed in **Table 2**. As described in the literature (Amin and Khaled., 2010; Yu et al., 2010; Li et al., 2011; Gerengi et al., 2016), copper corrosion reactions in chloride could be remarked as follows:

The anodic dissolution reactions are given as follows:

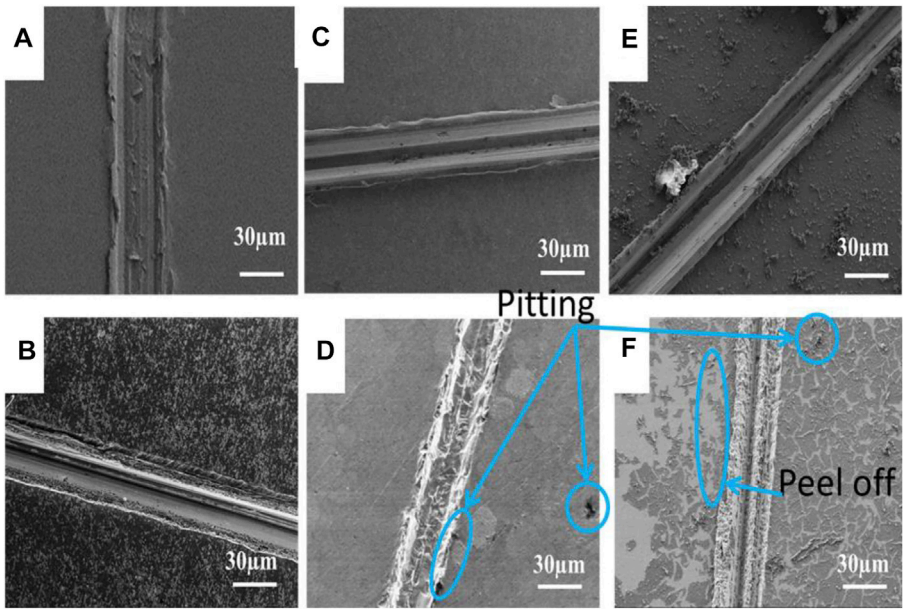

FIGURE 7 | SEM images of the scratched copper surfaces **(A)** bare Cu, **(C)** 0.02M 8-HQ@Cu, **(E)** PDA@Cu, and the corresponding scratched copper surfaces: **(B)** bare Cu, **(D)** 0.02M 8-HQ@Cu, and **(F)** PDA@Cu, taken after immersed in 3.5 wt.% NaCl aqueous solution for 10 h (corrosion time) at 25°C.

$$Cu \rightarrow Cu^{+} + e^{-}, \quad (1)$$

$$Cu^{+} + Cl^{-} \rightarrow CuCl, \quad (2)$$

$$CuCl + Cl^{-} \rightarrow CuCl_2 \quad (3)$$

$$CuCl_{2^{-}} \rightarrow + Cu^{2+}2Cl^{-} + e^{-}. \quad (4)$$

The cathodic oxygen reduction reaction is given as follows:

$$O_2 + 2H_2O + 4e^{-} \rightarrow 4OH^{-}. \quad (5)$$

By Tafel line extrapolation, the corrosion current density (j_{corr}), corrosion potential (E_{corr}), anodic Tafel slopes (β_a), and cathodic Tafel slopes (β_c) could be obtained. The j_{corr} value of the coated coppers is smaller than that of bare copper. The lowest j_{corr} could be reached at PDA@0.02M 8-HQ@Cu, which shows a decrease in magnitude by two orders, compared to bare copper (from 0.776 to 0.0071 μA). The results also suggest that the inhibition efficiency of the composite coating with 0.02 M 8-HQ exhibits the greatest resistance to salt corrosion, and the inhibition efficiency could reach 99.09%. In addition, all coatings retard both the cathodic and anodic reactions to some extent, and the differences in β_c are less noticeable than β_a. This indicates that after modified copper surface with PDA or PDA@8-HQ, the reduction of dissolved oxygen and the diffusion of $CuCl_2^{-}$ are diminished (Zucchi et al., 2004).

Electrochemical Impedance Spectroscopy

To evaluate the protective ability of the composite coating for copper, EIS is an effective method (King et al., 2014). **Supplementary Figure S4** shows the Nyquist plots of the coated copper electrodes in 3.5 wt.% NaCl solution, and the inset plot shows that of the bare copper. A capacitive loop in the high-frequency range could indicate the solution resistance, and a straight line in the low-frequency range, Warburg impedance, is associated with the diffusion of $CuCl_2^{-}$ (Babouri et al., 2015). After modification by PDA and PDA@8-HQ at the copper surfaces, in both EIS spectra, the Warburg impedances disappear and the radius of the capacitive loops increases. PDA@0.02M 8-HQ@Cu presents the highest impedance modulus.

In the Bode plots in **Figure 5A**, the impendence value at low frequency ($|Z|_{0.01Hz}$) increases from 3.48 to 5.16 with respect to bare copper. In the phase angle plots of **Figure 5B**, bare copper, PDA@Cu, and PDA@8-HQ@Cu have two time constants. PDA@0.02 M 8-HQ@Cu shows the maximum phase angle, manifesting the best inhibition efficiency. The result is in good consistency with that of potentiodynamic polarization.

For better understanding of the corrosion mechanism, ZsimpWin software was used to fit impedance spectra. The equivalent circuit model shows the minimum error and chi-square value (χ^2) less than 1×10^{-3}. The fitted electrical circuits are shown in **Figure 6**, and the corresponding electrochemical parameters are listed in **Table 3**. The most suitable fitting circuit model for bare copper is R(Q{R[Q(RW)]}), while the equivalent circuit model of R{Q[R(QR)]} is picked out for PDA@Cu. Additionally, R(QR)(QR) is a better mode for fitting the PDA@8-HQ coating. In the equivalent circuits, R_s stands for NaCl solution resistance, and R_{ct} and R_f represent charge transfer resistance and the resistance of the film, respectively. Constant phase elements (Q_c and Q_f) are with respect to copper oxide, PDA coating, and PDA@8-HQ coating. W is Warburg impedance. The Q impedance is defined as $Z_Q = Y_0^{-1} (j\omega)^{-n}$ (Shi et al., 2017), in which Y_0 is the values of Q, j is the imaginary number, ω ($\omega = 2\pi f$) is the angular frequency, and n is the phase ($-1 \leq n \leq 1$), which is related to the inhibitor adsorption, surface inhomogeneity, and porous layer formation. When n is −1, 0, 0.5, and 1, the Q

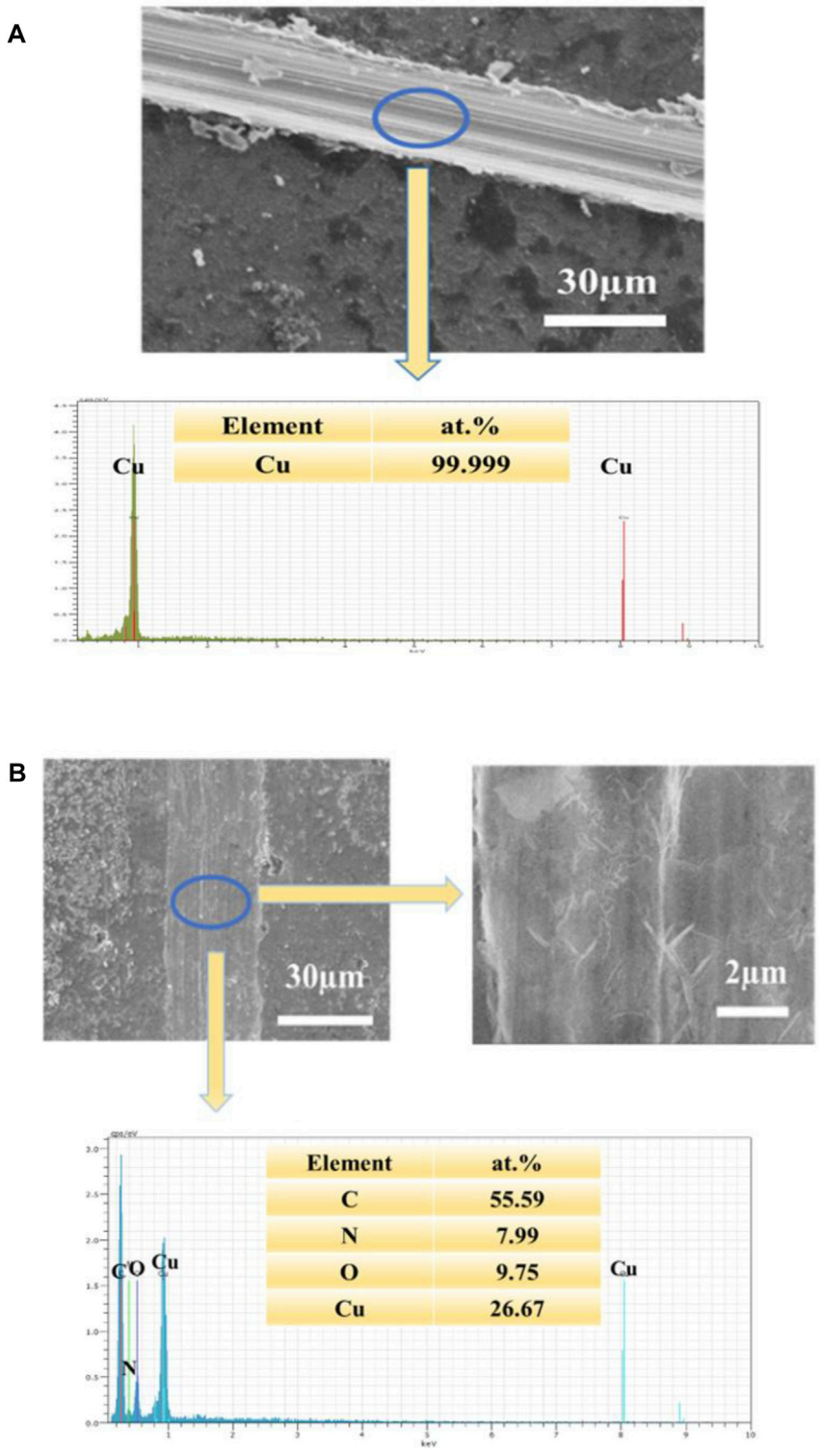

FIGURE 8 | (A): SEM image of the scratched PDA@0.02M 8-HQ@Cu and EDS spectrogram **(B)**: SEM image of the scratched PDA@0.02M 8-HQ@Cu and high magnification, immersed in 3.5 wt.% NaCl aqueous solution for 10 h (corrosion time) at 25°C, and EDS spectrogram.

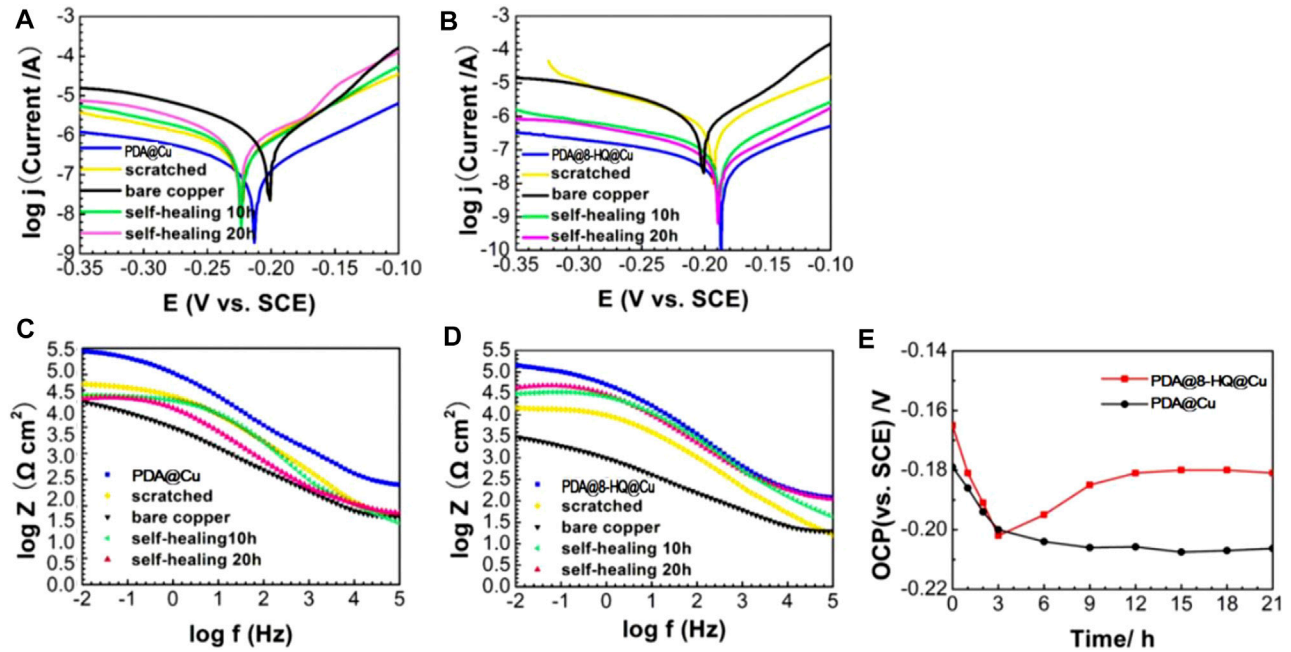

FIGURE 9 | Tafel **(A,B)** and Bode plots **(C,D)** recorded on the self-healing tests on scratched coatings of PDA@Cu and PDA@0.02M 8-HQ@Cu. **(E)** is OCP (vs. SCE) as a function of immersion time in 3.5 wt.% NaCl solution for scratched samples of PDA@Cu and PDA@0.02M 8-HQ@Cu.

TABLE 4 | Anticorrosion performance obtained from potentiodynamic polarization curves recorded with the self-healing tests on PDA@Cu and PDA@0.02 M 8-HQ@Cu samples.

Sample	$^{-}E_{corr}$ (V vs.·SCE)	j_{corr} (μA cm^{-2})	$^{-}\beta_c$ (V·dec^{-1})	β_a (V·dec^{-1})	η (%)
Bare copper	0.191 ± 0.002	0.776 ± 0.005	10.7 ± 0.86	23.1 ± 1.12	—
PDA	0.204 ± 0.004	0.129 ± 0.003	17.0 ± 1.51	18.7 ± 1.67	83.38
Scratched	0.222 ± 0.001	0.291 ± 0.003	21.6 ± 0.93	14.1 ± 0.74	62.50
Self-healing 10 h	0.223 ± 0.002	0.296 ± 0.002	21.0 ± 0.79	11.8 ± 0.82	61.86
Self-healing 20 h	0.225 ± 0.003	0.447 ± 0.004	18.6 ± 0.86	16.7 ± 1.01	42.40
PDA@0.02M 8-HQ	0.184 ± 0.003	0.007 ± 0.008	37.4 ± 1.73	97.2 ± 1.85	99.10
Scratched	0.189 ± 0.002	0.268 ± 0.002	21.9 ± 0.89	39.2 ± 0.79	65.46
Self-healing 10 h	0.185 ± 0.001	0.047 ± 0.005	19.5 ± 0.99	37.8 ± 0.93	93.94
Self-healing 20 h	0.184 ± 0.003	0.003 ± 0.004	19.6 ± 0.82	36.8 ± 1.05	99.61

TABLE 5 | Reproducibility of anticorrosion performance obtained from EIS measurements recorded with the self-healing tests on five different PDA@0.02M 8-HQ samples.

PDA@ 0.02M 8-HQ@Cu	R_s (Ω cm^2)	R_f (Ω cm^2)	Q_1 $Y_0 \times 10^{-4}$ (Ω^{-1} cm^{-2}·S^n)	n_1	Q_2 $Y_0 \times 10^{-4}$ (Ω^{-1} cm^{-2}·S^n)	n_2	R_{ct} (Ω cm^2)	R_p	RSD (%)
1	1.672	2,743	2.557	0.661	9.112	0.5195	327.58	3,070.58	2.69
2	1.885	2,413	4.655	0.6764	2.145	0.6721	570.4	2,983.4	
3	1.235	2,938	3.588	0.7124	3.483	0.7655	261.85	3,199.85	
4	1.899	2,590	2.589	0.6893	3.966	0.6254	452.79	3,042.79	
5	1.537	2,632	2.887	0.6989	2.717	0.7559	499.5	3,131.15	

represents inductance, resistance, Warburg impedance, and capacitance, respectively. As seen in **Table 3**, the n value of modified samples ranges from 0.5 to 1, meaning the relatively slow corrosion process (Li et al., 2014).

As for blank copper, R_f and Q_f are attributed to the inevitable layer of corrosion products (Refait et al., 2020). Nevertheless, diffusion in such a relatively thin layer then becomes possible, resulting in the presence of W. As for the PDA-modified copper

electrode, R_f and Q_f are caused by a composite film containing copper oxides and PDA. This thick PDA film therefore hinders the diffusion process causing W disappearance. For PDA@0.02M 8-HQ coating, since 8-HQ can fill the cracks of PDA, the dense protection layer shows the greatest inhibition efficiency up to 97.58%. Therefore, the first time constant is correlated with the film of PDA@0.02M 8-HQ coating, and the second time constant is then the double layer (Farahati et al., 2019).

SELF-HEALING BEHAVIOR

SEM Observations

Figure 7 shows FE-SEM images of copper with and without PDA or 8-HQ coatings, scratched by external forces, which were taken before and after corroded in 3.5 wt.% NaCl aqueous solution for 10 h. In **Figures 7B,D**, after immersion, there are many pitting corrosions that occurred at the scratched bare copper and the scratched 0.02M 8-HQ@Cu surface, and the visible corrosion products around the scratched spots indicate severe corrosion. Much seriously, in **Figure 7F**, the PDA coating has partly peeled off from the copper surface after long-term immersion in NaCl media. Obviously, the protection efficiencies of copper from corrosive solution by only PDA coating or 8-HQ are not satisfactory. **Figure 8A** shows SEM images and EDS results recorded before immersion of the scratched PDA@ 0.02M 8-HQ@Cu in salt solution. The exposure of copper in the scratched portion of PDA@ 0.02M 8-HQ@Cu could be visible.

In **Figure 8B** of scaled SEM images, after the scratched PDA@ 0.02M 8-HQ@Cu in 3.5 wt.% NaCl solution for 10 h, some nanorods produced in the vicinity of the scratched trace could be found, and the EDS result indicates that the nanorods are mainly composed of O, N, C, and Cu elements. **Supplementary Figure S5** shows the section views of the PDA@0.02M 8-HQ@Cu. After immersion in 3.5 wt.% NaCl aqueous solution for 10 h, nearly no corrosion occurred in the scratched portion due to the self-healing ability of composite coating. It shows that when the coating is damaged by external forces, 8-HQ embedded in the PDA coating would combine with copper ions through electrostatic attraction, forming insoluble clathrate of bis(8-hydroxyquinoline) copper [Cu $(HQ)_2$]. The preeminent self-healing ability of such PDA@0.02M 8-HQ composite coating will also be validated by following an electrochemical experiment.

Electrochemical Test

Potentiodynamic polarization was used to characterize self-healing property. PDA@Cu and PDA@0.02M 8-HQ@Cu were scratched with a knife, and then the scratched coatings were immersed in 3.5 wt.% NaCl solution for 0 h, 10 h, and 20 h. As shown in **Figures 9A,B** and **Table 4**, compared to the intact PDA@Cu and PDA@0.02M 8-HQ@Cu, j_{corr} values of both scratched coatings increased. However, j_{corr} value of the scratched PDA@Cu sample kept increasing with increasing immersion time, indicating further corrosion in NaCl aqueous solution. By contrast, for PDA@0.02M 8-HQ@Cu, j_{corr} value remarkably decreased (down to 0.003 μA cm^{-2}) as soaking time increased, and after self-healing for 20 h, the inhibition efficiency of the scratched PDA@0.02M 8-HQ@Cu recovered to the original level of the unscratched one.

Figures 9C,D show the Bode plots of self-healing tests of PDA@Cu and PDA@0.02M 8-HQ@Cu. At the beginning stage, the impendence values at low frequency for scratched PDA@Cu and PDA@0.02M 8-HQ@Cu reduce an order of magnitude compared to undamaged coatings. Similarly, after self-healing for 20 h, the impendence value of scratched PDA@0.02M 8-HQ@Cu increased to the same level as the unscratched coating, hinting that the scratches have been repaired by 8-HQ molecules. By contrast, in the case of scratched PDA@Cu, the impendence value decreased with the time undergoing. From **Table 5**, EIS measurements with RSD about 2.69% repeated for five batches of scratched samples reveal excellent reproducibility. **Figure 9E** shows OCP (vs. SCE) curves for scratched PDA@Cu and scratched PDA@0.02M 8-HQ@Cu in 3.5 wt.% NaCl solution over the immersion time. Both OCP values (vs. SCE) of scratched PDA@Cu and scratched PDA@0.02M 8-HQ@Cu present a sharp fall in the first 3 h, indicating corrosion occurrence in the cracks by the penetration of the corrosive media. After 3 h, OCP (vs. SCE) of scratched PDA@Cu remained decreased, while OCP (vs. SCE) of scratched PDA@0.02M 8-HQ@Cu increased due to the self-healing behavior. After 12 h, the OCP value of scratched PDA@0.02M 8-HQ coating reached 181 mV (vs. SCE), which was close to the undamaged coating (ca. 172 mV). The self-healed coating exhibited a stable protection performance for the copper substrate after immersion in salt solution for 20 h.

CONCLUSION

In summary, a facile strategy to prepare a protection coating with self-healing capability was proposed. We first constructed a composite coating at the copper surface by embedding inhibitor of 8-HQ into the PDA coating by using the one-step method. Under an optimal formation of the composite coating by using 8-HQ at 0.02 M, the suppression efficiency of about 99.1% can be reached. PDA@0.02M 8-HQ@Cu not only showed the efficient inhibition of corrosion but also demonstrated the self-healing ability in case of mechanical damage. By scratching PDA@0.02M 8-HQ@Cu electrode, the inhibitor in the composite coating will be exposed, and Cu (II) will electrostatically adsorb with 8-HQ and complex to seal the cracks caused by scratching to produce the complexation, which sufficiently inhibits corrosion occurring in the scratched trace. After 20 h of self-healing, the inhibition efficiency reached 99.61%.

PERMISSION TO REUSE AND COPYRIGHT

DATA AVAILABILITY STATEMENT

The original contributions presented in the study are included in the article/**Supplementary Material**, further inquiries can be directed to the corresponding authors.

AUTHOR CONTRIBUTIONS

JF and WC: conceptualization and writing/original draft preparation; YJ and SL: investigation and numeral calculations; and HY and YY: writing—review and editing. All the authors contributed to the article and approved the submitted version.

FUNDING

This research is funded by the National Natural Science Foundation of China (No. 21707091).

ACKNOWLEDGMENTS

We greatly appreciate the support of the National Natural Science Foundation of China (No. 21707091), Joint International Research Laboratory of Resource Chemistry, Ministry of Education, Shanghai Key Laboratory of Rare Earth Functional Materials, Key Laboratory of Resource Chemistry of Ministry of Education, "111" Innovation and Talent Recruitment Base on Photochemical and Energy Materials (No. D18020), Shanghai Engineering Research Center of Green Energy Chemical Engineering (No. 18DZ2254200), and Shanghai Municipal Education Committee Key Laboratory of Molecular Imaging Probes and Sensors.

SUPPLEMENTARY MATERIAL

The Supplementary Material for this article can be found online at: https://www.frontiersin.org/articles/10.3389/fmats.2022.850362/full#supplementary-material

REFERENCES

Albini, M., Letardi, P., Mathys, L., Brambilla, L., SchröterJunierbJoseph, J. P. E., Junier, P., et al. (2018). Comparison of a Bio-Based Corrosion Inhibitor versus Benzotriazole on Corroded Copper Surfaces. *Corrosion Sci.* 143, 84–92. doi:10.1016/j.corsci.2018.08.020

Amin, M. A., and Khaled, K. F. (2010). Copper Corrosion Inhibition in O2-Saturated H2SO4 Solutions. *Corrosion Sci.* 52, 1194–1204. doi:10.1016/j.corsci.2009.12.035

Babouri, L., Belmokre, K., Abdelouas, A., Bardeau, J-F., and El Mendili, Y. (2015). The Inhibitive Effect of Cerium Carbonate on the Corrosion of Brass in 3% NaCl Solution. *Int. J. Electrochem. Sci.* 10, 7818–7839.

Bernsmann, F., Ball, V., Addiego, F., Ponche, A., Michel, M., Gracio, J. J. D. A., et al. (2011). Dopamine–Melanin Film Deposition Depends on the Used Oxidant and Buffer Solution. *Langmuir* 27, 2819–2825. doi:10.1021/la104981s

Behzadnasab, M., Mirabedini, S. M., Esfandeh, M., and Farnood, R. R. (2017). Evaluation of Corrosion Performance of a Self-Healing Epoxy-Based Coating Containing Linseed Oil-Filled Microcapsules via Electrochemical Impedance Spectroscopy. *Prog. Org. Coat.* 105, 212–224. doi:10.1016/j.porgcoat.2017.01.006

Caldas, C. M., Calheiros, L. F., and G. Soares, B. (2017). Silica-polyaniline Hybrid Materials Prepared by Inverse Emulsion Polymerization for Epoxy-Based Anticorrosive Coating. *J. Appl. Polym. Sci.* 134, 45505–45513. doi:10.1002/app.45505

Chen, T., Chen, R., Jin, Z., and Liu, J. (2015). Engineering Hollow Mesoporous Silica Nanocontainers with Molecular Switches for Continuous Self-Healing Anticorrosion Coating. *J. Mater. Chem. A.* 3, 9510–9516. doi:10.1039/c5ta01188d

Cheng, Y., Wu, B., Ma, X., Lu, S., Xu, W., Szunerits, S., et al. (2018). Facile Preparation of High Density Polyethylene Superhydrophobic/superoleophilic Coatings on Glass, Copper and Polyurethane Sponge for Self-Cleaning, Corrosion Resistance and Efficient Oil/water Separation. *J. Colloid Interf. Sci.* 525, 76–85. doi:10.1016/j.jcis.2018.04.075

Chou, C.-C., Hsin, S.-W., Lin, H.-C., Yeh, C.-H., Wu, R., and Cherng, W.-J. (2016). Oxidized Dopamine as the Interlayer between Heparin/collagen Polyelectrolyte Multilayers and Titanium Substrate: An Investigation of the Coating's Adhesion and Hemocompatibility. *Surf. Coat. Technol.* 303, 277–282. doi:10.1016/j.surfcoat.2016.03.098

Cui, L.-Y., Gao, S.-D., Li, P.-P., Zeng, R.-C., Zhang, F., Li, S.-Q., et al. (2017). Corrosion Resistance of a Self-Healing Micro-arc Oxidation/polymethyltrimethoxysilane Composite Coating on Magnesium alloy AZ31. *Corrosion Sci.* 118, 84–95. doi:10.1016/j.corsci.2017.01.025

Daradmare, S., Pradhan, M., Raja, V. S., and Parida, S. (2016). Encapsulating 8-hydroxyquinoline in Graphene Oxide-Stabilized Polystyrene Containers and its Anticorrosion Performance. *J. Mater. Sci.* 51, 10262–10277. doi:10.1007/s10853-016-0254-4

Farahati, R., Ghaffarinejad, A., Rezania, H., Mousavi-Khoshdel, S. M., and Behzadi, H. (2019). Sulfonated Aromatic Polyamide as Water-Soluble Polymeric Corrosion Inhibitor of Copper in HCl. *Colloids Surf. A: Physicochemical Eng. Aspects* 578, 123626. doi:10.1016/j.colsurfa.2019.123626

Feng, Y., Feng, L., Sun, Y., and He, J. (2020). The Inhibition Mechanism of a New Synthesized Indole Derivative for Copper in Acidic Environment via Experimental and Theoretical Study. *J. Mater. Res. Technol.* 9 (1), 584–593. doi:10.1016/j.jmrt.2019.10.087

Gerengi, H., Mielniczek, M., Gece, G., and Solomon, M. M. (2016). Experimental and Quantum Chemical Evaluation of 8-Hydroxyquinoline as a Corrosion Inhibitor for Copper in 0.1 M HCl. *Ind. Eng. Chem. Res.* 55, 9614–9624. doi:10.1021/acs.iecr.6b02414

Grigoriev, D., Shchukina, E., and Shchukin, D. G. (2017). Nanocontainers for Self-Healing Coatings. *Adv. Mater. Inter.* 4, 1600318–1600328. doi:10.1002/admi.201600318

Hou, B., Li, X., Ma, X., Du, C., Zhang, C. D., Zheng, M., et al. (2017). The Cost of Corrosion in China. *NPJ Mater. Degrad.* 1, 4. doi:10.1038/s41529-017-0005-2

Jiang, J., Zhu, L., Zhu, L., Zhang, H., Zhu, B., and Xu, Y. (2013). Antifouling and Antimicrobial Polymer Membranes Based on Bioinspired Polydopamine and Strong Hydrogen-Bonded Poly(N-Vinyl Pyrrolidone). *ACS Appl. Mater. Inter.* 5, 12895–12904. doi:10.1021/am403405c

Jiang, Y. Y., Li, S. T., Fan, J. J., Liu, Z. Q., Guo, X. Y., Yin, Y., et al. (2021). Functionalized Multi-Walled Carbon Nanotubes Reinforced Coating for Metal protection. *J. Shanghai Normal Univ. (Natural Sciences)* 50 (05), 517–527. doi:10.3969/J.ISSN.1000-5137.2021.05.001

Jing, C., Wang, Z., Gong, Y., Huang, H., Ma, Y., Xie, H., et al. (2018). Photo and Thermally Stable Branched Corrosion Inhibitors Containing Two Benzotriazole Groups for Copper in 3.5 Wt% Sodium Chloride Solution. *Corros. Sci.* 138, 353–357. doi:10.1016/j.corsci.2018.04.027

Johansen, H. D., Brett, C. M. A., and Motheo, A. J. (2012). Corrosion protection of Aluminium alloy by Cerium Conversion and Conducting Polymer Duplex Coatings. *Corrosion Sci.* 63, 342–350. doi:10.1016/j.corsci.2012.06.020

King, A. D., Birbilis, N., and Scully, J. R. (2014). Accurate Electrochemical Measurement of Magnesium Corrosion Rates; a Combined Impedance, Mass-Loss and Hydrogen Collection Study. *Electrochimica Acta* 121, 394–406. doi:10.1016/j.electacta.2013.12.124

Li, W., Hu, L. C., Zhang, S. G., and Hou, B. R. (2011). Effects of Two Fungicides on the Corrosion Resistance of Copper in 3.5% NaCl Solution under Various Conditions. *Corros. Sci.* 53, 735–745. doi:10.1016/j.corsci.2010.11.006

Li, G. L., ZhengMöhwald, Z. H., Möhwald, H., and Shchukin, D. G. (2013). Silica/Polymer Double-Walled Hybrid Nanotubes: Synthesis and Application as Stimuli-Responsive Nanocontainers in Self-Healing Coatings. *ACS Nano* 7, 2470–2478. doi:10.1021/nn305814q

Li, C. C., Guo, X. Y., Shen, S., Song, P., Xu, T., Wen, Y., et al. (2014). Adsorption and Corrosion Inhibition of Phytic Acid Calcium on the Copper Surface in 3 Wt% NaCl Solution. *Corros. Sci.* 83, 147–154. doi:10.1016/j.corsci.2014.02.001

Li, J., Feng, Q., Cui, J., Yuan, Q., Qiu, H., Gao, S., et al. (2017). Self-assembled Graphene Oxide Microcapsules in Pickering Emulsions for Self-Healing Waterborne Polyurethane Coatings. *Composites Sci. Technol.* 151, 282–290. doi:10.1016/j.compscitech.2017.07.031

Li, J., Wang, R., Zhang, D., Su, Z., Li, H., and Yan, Y. (2019). Copper Iodide (CuI) Coating as a Self-Cleaning Adsorbent for Highly Efficient Dye Removal. *J. Alloys Compd.* 774, 191–200. doi:10.1016/j.jallcom.2018.09.373

Liu, Y., Wang, L., Zhang, C., Zhang, K., and Liu, G. (2013). A Hollow Porous Mn2O3 Microcontainer for Encapsulation and Release of Corrosion Inhibitors. *ECS Electrochemistry Lett.* 2, C39–C42. doi:10.1149/2.003310eel

Luo, X., and Mather, P. T. (2013). Shape Memory Assisted Self-Healing Coating. *ACS Macro Lett.* 2, 152–156. doi:10.1021/mz400017x

Mahmoud, M. E., Haggag, S. S., and Abdel-Fattah, T. M. (2009). Surface Layer-By-Layer Chemical Deposition Reaction for Thin Film Formation of Nano-Sized Metal 8-hydroxyquinolate Complexes. *Polyhedron* 28, 181–187. doi:10.1016/j.poly.2008.09.030

Mahmoudian, M., Nozad, E., Kochameshki, M. G., and Enayati, M. (2018). Preparation and Investigation of Hybrid Self-Healing Coatings Containing Linseed Oil Loaded Nanocapsules, Potassium Ethyl Xanthate and Benzotriazole on Copper Surface. *Prog. Org. Coat.* 120, 167–178. doi:10.1016/j.porgcoat.2018.03.014

Nestorson, A., Forsgren, G., Leufvén, A., and Järnström, L. (2007). Multivariate Analysis of Retention and Distribution of Aroma Compounds in Barrier Dispersion Coatings. *Packag. Technol. Sci.* 20, 345–358. doi:10.1002/pts.765

Park, J.-H., and Braun, P. V. (2010). Coaxial Electrospinning of Self-Healing Coatings. *Adv. Mater.* 22, 496–499. doi:10.1002/adma.200902465

Qian, H., Xu, D., Du, C., Zhang, D., Li, X., Huang, L., et al. (2017). Dual-action Smart Coatings with a Self-Healing Superhydrophobic Surface and Anti-corrosion Properties. *J. Mater. Chem. A.* 5, 2355–2364. doi:10.1039/c6ta10903a

Qiang, Y., Fu, S., Zhang, S., Chen, S., and Zou, X. (2018). Designing and Fabricating of Single and Double Alkyl-Chain Indazole Derivatives Self-Assembled Monolayer for Corrosion Inhibition of Copper. *Corrosion Sci.* 140, 111–121. doi:10.1016/j.corsci.2018.06.012

Refait, P., Rahal, C., and Masmoudi, M. (2020). Corrosion Inhibition of Copper in 0.5 M NaCl Solutions by Aqueous and Hydrolysis Acid Extracts of Olive Leaf. *J. Electroanalytical Chem.* 859, 113834. doi:10.1016/j.jelechem.2020.113834

Shi, H., Wu, L., Wang, J., Liu, F., and Han, E.-H. (2017). Sub-micrometer Mesoporous Silica Containers for Active Protective Coatings on AA 2024-T3. *Corrosion Sci.* 127, 230–239. doi:10.1016/j.corsci.2017.08.030

Sumerlin, B. S. (2018). Next-generation Self-Healing Materials. *Science* 362, 150–151. doi:10.1126/science.aau6453

Tavandashti, N. P., Ghorbani, M., Shojaei, A., Mol, J. M. C., Terryn, H., Baert, K., et al. (2016). Inhibitor-loaded Conducting Polymer Capsules for Active Corrosion protection of Coating Defects. *Corrosion Sci.* 112, 138–149. doi:10.1016/j.corsci.2016.07.003

Wan, Y., Chen, M., Liu, W., Shen, X., Min, Y., and Xu, Q. (2018). The Research on Preparation of Superhydrophobic Surfaces of Pure Copper by Hydrothermal Method and its Corrosion Resistance. *Electrochimica Acta* 270, 310–318. doi:10.1016/j.electacta.2018.03.060

Xu, J.-B., Cao, Y.-Q., Fang, L., and Hu, J.-M. (2018). A One-step Preparation of Inhibitor-Loaded Silica Nanocontainers for Self-Healing Coatings. *Corrosion Sci.* 140, 349–362. doi:10.1016/j.corsci.2018.05.030

Xu, C., Shan, Y., Bilal, M., Xu, B., Cao, L., and Huang, Q. (2020). Copper Ions Chelated Mesoporous Silica Nanoparticles via Dopamine Chemistry for Controlled Pesticide Release Regulated by Coordination Bonding. *Chem. Eng. J.* 395, 125093. doi:10.1016/j.cej.2020.125093

Yu, F., Chen, S., Chen, Y., Li, H., Yang, L., Chen, Y., et al. (2010). Experimental and Theoretical Analysis of Polymerization Reaction Process on the Polydopamine Membranes and its Corrosion protection Properties for 304 Stainless Steel. *J. Mol. Struct.* 982, 152–161. doi:10.1016/j.molstruc.2010.08.021

Zhang, D., Lu, J., Shi, C., Zhang, K., Li, J., and Gao, L. (2021). Anti-corrosion Performance of Covalent Layer-By-Layer Assembled Films via Click Chemistry Reaction on the Copper Surface. *Corrosion Sci.* 178, 109063. doi:10.1016/j.corsci.2020.109063

Zhang, K., Wang, L., and Liu, G. (2013). Copper(II) 8-hydroxyquinolinate 3D Network Film with Corrosion Inhibitor Embedded for Self-Healing Corrosion protection. *Corrosion Sci.* 75, 38–46. doi:10.1016/j.corsci.2013.05.014

Zhang, Z., Zhang, J., Zhang, B., and Tang, J. (2013). Mussel-inspired Functionalization of Graphene for Synthesizing Ag-Polydopamine-Graphenenanosheets as Antibacterial Materials. *Nanoscale* 5, 118–123. doi:10.1039/c2nr32092d

Zhao, Y., Wang, H., Qian, B., Li, H., and Ren, F. (2018). Copper-polydopamine Composite Derived from Bioinspired Polymer Coating. *J. Alloys Compd.* 742, 191–198. doi:10.1016/j.jallcom.2018.01.183

Zhao, Y., Wu, Z., Di Carlo, F., Li, H., Qian, B., Feng, Z., et al. (2019). Enhancing the Electrical and Mechanical Properties of Copper by Introducing Nanocarbon Derived from Polydopamine Coating. *J. Alloys Compd.* 778, 288–293. doi:10.1016/j.jallcom.2018.11.145

Zucchi, F., Grassi, V., Frignani, A., and Trabanelli, G. (2004). Inhibition of Copper Corrosion by Silane Coatings. *Corrosion Sci.* 46, 2853–2865. doi:10.1016/j.corsci.2004.03.019

Conflict of Interest: The authors declare that the research was conducted in the absence of any commercial or financial relationships that could be construed as a potential conflict of interest.

Publisher's Note: All claims expressed in this article are solely those of the authors and do not necessarily represent those of their affiliated organizations, or those of the publisher, the editors, and the reviewers. Any product that may be evaluated in this article, or claim that may be made by its manufacturer, is not guaranteed or endorsed by the publisher.